Available online at www.sciencedirect.com
ScienceDirect
Journal of Nuclear Materials 360 (2007) 151–158
journal of nuclear materials
www.elsevier.com/locate/jnucmat

# Comparative study and imaging by PhotoElectroChemical techniques of oxide films thermally grown on zirconium and Zircaloy-4

R. Benaboud [a], P. Bouvier [b], J.-P. Petit [b], Y. Wouters [a,*], A. Galerie [a]

[a] *Laboratoire de Thermodynamique et de Physico-Chimie Métallurgiques, UMR INPG/CNRS/UJF 5614, 1130 rue de la Piscine, F-38402 Saint-martin d'Hères cedex, France*
[b] *Laboratoire d'Electrochimie et de Physico-chimie des Matériaux et des Interfaces, UMR INPG/CNRS/UJF 5631, Ecole Nationale Supérieure d'Electrochimie et d'Electrométallurgie de Grenoble, Institut National Polytechnique de Grenoble, F-38402 Saint-martin d'Hères cedex, France*

Received 7 April 2006; accepted 2 October 2006

**Abstract**

The oxidation of iron and chromium that are present as impurities in zirconium metal or as alloying elements in Zircaloy-4 was investigated with PhotoElectroChemical techniques (PEC), highlighting the chemical nature, the size and the lateral distribution of Fe and Cr-containing phases in thin zirconia scales formed during the oxidation of pure zirconium and Zircaloy-4 at 470 °C in oxygen. In the case of zirconium, iron and chromium impurities led to the formation of oxides distributed in a homogeneous way in the zirconia scale, while in the case of Zircaloy-4 these elements, present in the form of intermetallic particles in the substrate, led to the formation of localised haematite $Fe_2O_3$, rhomboedric solid solution $(Fe_xCr_{1-x})_2O_3$ and chromia $Cr_2O_3$ phases. These phases were accurately studied via the measurement of their respective band-gap ($Fe_2O_3$: 2.2 eV, $(Fe_xCr_{1-x})_2O_3$: 2.6 eV and $Cr_2O_3$: 3.0 eV). It is concluded that PEC techniques represent a sensitive and powerful way to locally analyse the various semiconductor phases in the oxide scale at a micron scale.


*PACS:* 81.00

## 1. Introduction

Zirconium alloys (Zircaloy-2, Zircaloy-4 and more recently M5) are materials widely used in the nuclear power industry. Indeed they present good mechanical properties and workability, with a remarkable corrosion resistance. Zircaloy-4, the most used and studied, is made from an α–Zr matrix with Sn in solid solution and intermetallic particles containing the other minor alloying elements Fe and Cr. These intermetallic precipitates are about 0.1–1.0 μm in diameter, depending on the fabrication conditions. The properties of these intermetallics have been studied for over two decades mainly using electron microscopy techniques, but the determination of volume fractions of the different phases by TEM has proven to be difficult. Moreover, the

* Corresponding author.
*E-mail address:* yves.wouters@ltpcm.inpg.fr (Y. Wouters).

0022-3115/$ - see front matter © 2006 Elsevier B.V. All rights reserved.
doi:10.1016/j.jnucmat.2006.10.001

evolution of these intermetallic precipitates during oxidation of the zirconium alloy was little studied and is still controversial. Some authors claim that $Zr(Fe,Cr)_2$ precipitates oxidise in service [1] while others affirm that they remain unoxidised in the oxide film [2]. It was even assumed by Pêcheur et al. [3] that precipitates remain unoxidised in the inner part of the zirconia scale while they oxidise in the outer part where the oxygen chemical potential is high enough. In the present study, we are mainly interested in understanding how alloying elements, such as iron and chromium, oxidize during the formation of thermal oxide scales on Zircaloy-4. For this purpose we used the Photo-ElectroChemical technique (PEC) which is known to be a valuable tool for investigating semi conducting materials in terms of electro-optical properties, more or less directly related to the chemical composition and structure of the material [4–9].

In the large number of studies published on the electrochemical behaviour of zirconium, only a limited number concern the PEC behaviour of zirconium oxide films. In these studies, $ZrO_2$ was mainly prepared by anodic oxidation, very seldom by thermal oxidation. The growth kinetics [10–14], electrical, optical and structural properties of films [14–21] were described in detail. Based on PEC experiments, the authors have assessed n-type semiconducting behaviour for thin anodic oxides and thicker thermal oxides [15,16,22], but they diverged on the value of band-gap energy of oxides. Burleigh et al. [23] found a band-gap of 3.8–3.9 eV for anodic Zr oxide films grown in $H_2SO_4$ 1 M and in KOH 1 M, while Goossens et al. [24] (in $H_3PO_4$ 1 M), Preusser et al. [25] (in $H_2SO_4$ 0.5 M) and Di Quarto et al. [26] (in solutions at pH in the range 0.3–13) claimed values of 4.50 to 4.87 eV for forbidden band-gap energies. With regard to the oxide films structure, several authors proposed that anodic zirconia films were made of only one layer. However, Di Quarto et al. [10,26] proposed a duplex structure, composed of a hydrated external phase $ZrO_2(H_2O)_n$ with a band-gap in the range 2.8–3.3 eV depending on the degree of hydration, and a $ZrO_2$ anhydrous internal phase with a higher band-gap (4.65 eV). The same assumption of a hydrated external layer was also suggested by Khalil et al. [12] by studying ionic transport in the scale. The duplex scale concept was also used to explain frequency dispersions in capacity measurements or ellipsometric results [14–19].

Contrary to pure zirconium, only a few articles were published on PEC characterisation of zirconium alloys. On Zircaloy-4, Lee et al. [27] showed that the formed oxide was composed of single or duplex layers depending on film formation potential, applied potential and polarisation time. Three different band-gap energies were found and interpreted as originating from an outer hydrated $ZrO_2$ layer with an electron transition at 2.9 eV, a localised electronic state at 3.2 eV, and an inner anhydrous $ZrO_2$ layer with an electron transition at 4.4 eV close to the value of crystalline thermal $ZrO_2$ layer formed in air at 400 °C.

In conclusion, the bibliography clearly shows that zirconia is a n-type semiconductor with a band-gap varying between 4 and 5 eV. Additional values in the range 2.2–3.5 eV show evidence of other semiconductor phases, not clearly identified. The question which remains unanswered is the participation of the alloying elements in these phases. The present study was focused on these addition elements, in order to assess their oxidation state in thermal zirconia films. In particular, it was important to check if the low-energy contributions described in the literature were due to a Zr oxide or to iron and/or chromium containing phases. In the first part of the paper, various band-gap energies are determined by macroscopic PEC measurements, in the second part, a microscopic PEC study is carried out to obtain the lateral distribution of the phases.

## 2. Experimental

### 2.1. Oxidation procedure

Zirconium metal, 99.8% in purity, was supplied by Goodfellow Metals Ltd. (ZR000320) and Zircaloy-4 alloy by CEZUS, FRAMATOME-ANP group (see Table 1). Samples in the form of 1 mm thick sheets and with dimensions $15 \times 15$ mm were SiC ground up to the grade 2400, then diamond polished to 1 μm. After cleaning and rinsing, they were isothermally oxidised in a microthermobalance at 470 °C. Oxygen at 150 mbar pressure in dynamic conditions was used as oxidising gas. The thickness of the formed scales was determined from the weight gain measurements, neglecting oxygen dissolved into the metal and considering that the major product of oxidation was monoclinic $ZrO_2$ (Table 2).

### 2.2. Macroscopic PhotoElectroChemical set-up

Macroscopic PEC measurements were obtained by illuminating the whole surface (area: 0.785 $cm^2$)

Table 1
Chemical composition (wt%) of the 'pure' zirconium samples (from Goodfellow Metals Ltd.) and of the Zircaloy-4 samples (from CEZUS)

| | % Sn | % C | % Hf | % Fe | % Cr | % N | % O | % H |
|---|---|---|---|---|---|---|---|---|
| 'Pure' zirconium | 0 | 0.025 | 0.25 | 0.02 | 0.02 | 0.01 | 0.1 | 0.001 |
| Zircaloy-4 | 1.3 | 0.012 | – | 0.2 | 0.1 | 0.03 | 0.13 | 0.001 |

Table 2
Thicknesses of the scales formed after 1 h oxidation at 470 °C in oxygen

| | |
|---|---|
| 'Pure' zirconium | 1.35 μm |
| Zircaloy-4 | 0.70 μm |

of the oxidised samples used as working electrodes in a classical three-electrodes electrochemical cell (see Fig. 1) equipped with a flat quartz optical window, using a platinum foil (area = 1 $cm^2$) as the counter electrode and a $Hg/Hg_2SO_4$ mercury sulphate electrode (MSE) as the reference electrode (+0.650 V/ENH). Electrical back contact was taken directly on the zirconium metal after removing the oxidation layer. The electrochemical cell was controlled by means of a Voltalab 32 potentiostat (Radiometer Analytical) driven by a home made software.

Photocurrent vs. energy curves were measured under modulated light conditions, using a lock-in amplifier (PAR 5208, EG&G Instruments) together with a mechanical light chopper (PAR 197, EG&G Instruments, $f = 21$ Hz), at variable wavelength using a 1000 W Xenon arc bulb (Müller GmbH Lax 1000) and a triple grating monochromator (PAR 1235, EG& G Instruments) allowing to select the photon wavelengths with a spectral width of ±1 nm.

To extract the quantum yield from the as-measured photocurrent values, a calibrated silicon photodiode (Hamamatsu S-1722) was used to measure the photon flux as a function of wavelength. For this purpose, the silicon photodiode replaced the sample in identical position after removing part of the electrolyte from the cell until the sample surface was grazing the surface of the electrolyte. This minimised the unavoidable uncertainties in the determination of the relative photon flux (and quantum yield) at each wavelength, as could be verified by comparing the transmission curves of colored solutions measured by means of either the photodiode or an UV–Visible spectrometer. In this study, quantum yield will be named photocurrent ($I^*_{phot}$).

All experiments were performed in an aqueous solution of sodium sulfate (0.1 M) at pH 8.0 ± 0.1. This electrolyte was continuously desaerated by argon bubbling.

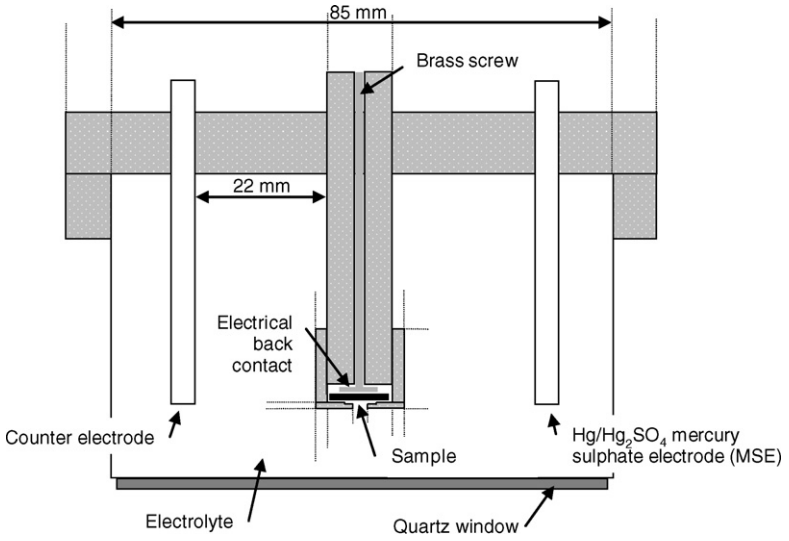


Fig. 1. Schematic representation of the electrochemical cell.

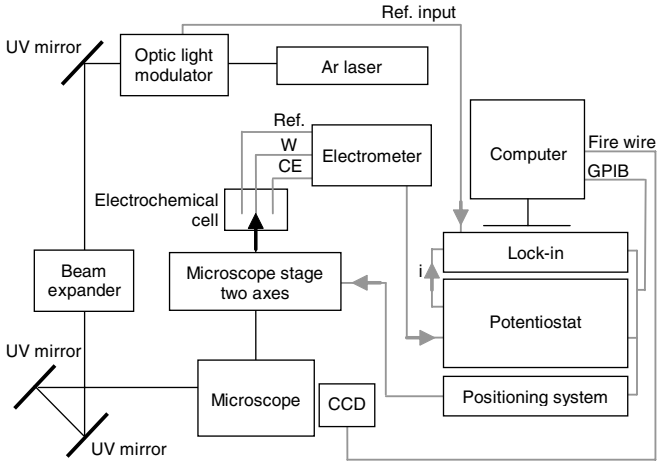


Fig. 2. Schematic representation of the micro PEC set-up.

### 2.3. Microscopic PhotoElectroChemical set-up

A schematic representation of the laboratory built microscopic PEC device used is presented in Fig. 2. The photocurrent was generated using a modulated ($f = 21$ Hz) monochromatic light from an Argon laser (Innova 90 C-A6 from Coherent, delivering four main lines: $E = 2.41$ eV, 2.73 eV, 3.51 eV, 3.72 eV). The beam was focused onto the surface of the oxidised sample to be studied via the objective of an inverted microscope (Olympus IX71, spot size ~1 μm). The image was built by moving the sample placed on a high resolution XY motorised Marzhauser microscope stage (Scan IM120 × 100). The same electrochemical cell as in the macroscopic PhotoElectroChemical set-up was used.

The lock-in technique was applied to separate the photocurrent from the total electrochemical current. For that purpose, the current output of the potentiostat (PAR 273 A, EG&G Instruments) was connected to the signal input of the lock-in amplifier (Stanford Research SR830) and the trigger signal of the optic light modulator (PAR 197, EG&G Instruments, $f = 21$ Hz) was fed to the reference input of the lock-in amplifier. A PEC image could be obtained at a given applied potential, by recording for each position of the sample surface, the amplitude and the phase of the photocurrent. The investigated area was selected on the optical image provided by a CCD camera. In the present experiments, various points spaced along the $X$ and $Y$ directions were used from 2 μm to 3 μm, leading to images with possible different resolutions. The whole of the instrumentation was controlled by a home-made software.

In the investigated laser power range (typically 1–10 mW), all measured photocurrents were proportional to the photon flux, indicating that charge transfer to the electrolyte was not the limiting step of photocurrent generation. To easily compare several images recorded at various light energies, all images are presented in the following at a given constant photon flux of $1 \times 10^{16}$ photon $s^{-1}$. The scale of the photocurrent, in these conditions, is in the range 0–40 nA.

In addition, the absorption index ($\alpha_\lambda$) depends on the investigated material but also on the incident energy. For zirconia, literature data [28–30] lead to light penetration depth ($1/\alpha_\lambda$) larger than the thicknesses of the considered oxide scales (see Table 2) in the used energy range (2–5.0 eV). Thus we consider that the incident light will interest the whole scale for all the considered energies.

## 3. Results and discussion

Two different oxide scales were prepared by oxidising 'pure' zirconium and Zircaloy-4 at 470 °C during 1 h in oxygen. As shown in Fig. 3, the X-ray diffraction patterns recorded on both samples could not attest for the presence of any other phases than monoclinic zirconia $ZrO_2$ polymorph ($P21/c$, $Z = 4$) and the underlying zirconium metal substrate. Macroscopic PEC spectra obtained on both samples, i.e. pure zirconium and Zircaloy-4, presented in Fig. 4 were normalised to the maximum photocurrent measured at 5.35 eV. Both spectra

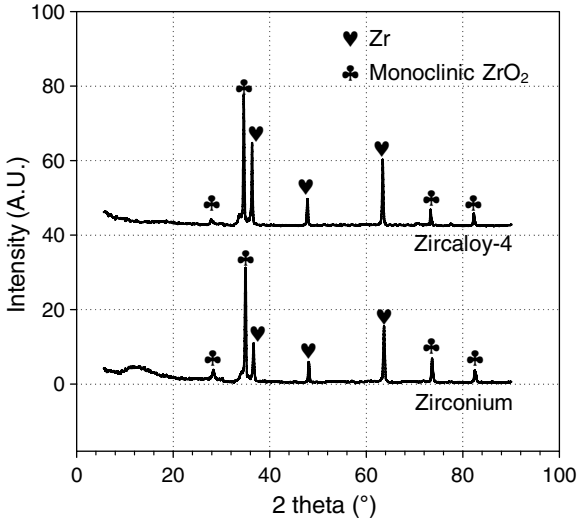


Fig. 3. XRD spectrum of 'pure' zirconium and Zircaloy-4 oxidised at 470 °C during 1 h.

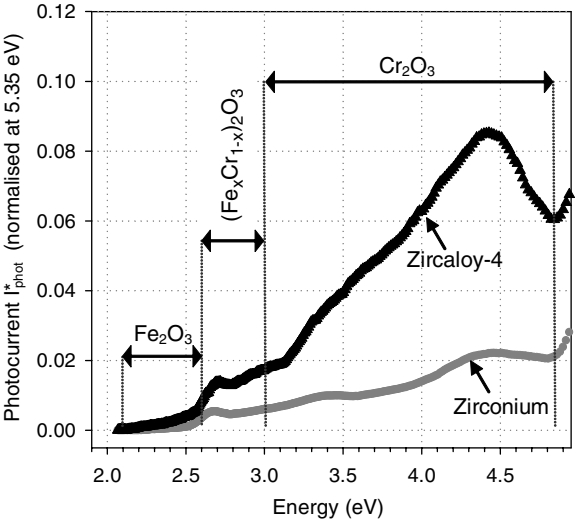


Fig. 5. Low energy photocurrent $I^*_{phot}$ spectra of the oxide scales grown at 470 °C during 1 h in oxygen on 'pure' zirconium and Zircaloy-4 (applied potential: 0 V/MSE).

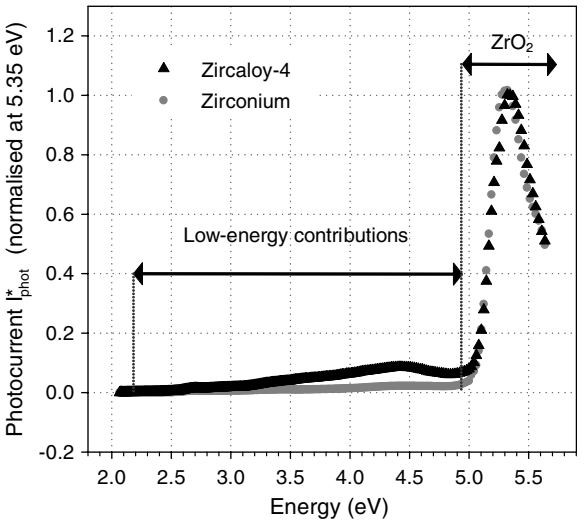


Fig. 4. Photocurrent $I^*_{phot}$ vs. light energy spectra of the oxide scales grown at 470 °C during 1 h in oxygen on 'pure' zirconium and Zircaloy-4 (applied potential: 0 V/MSE).

exhibited a major contribution at the high energy onset of 5 eV, value in good agreement with the known one for the band-gap of monoclinic zirconia [26,31–33], confirming the X-ray diffraction analysis and the presence of this phase as the major one in the two different oxide scales. Moreover, the detail of the low energy region of these spectra presented in Fig. 5, revealed more complex information due to the presence of several other contributions between 2 and 4.5 eV. It must be pointed out that these contributions displayed identical energy dependence (same shape), highlighting that the origins of the latter ones were probably the same for both materials. However, higher photocurrent values were measured on Zircaloy-4 compared to pure zirconium. At the same time, the respective iron and chromium impurities contents found in zirconium (0.02%Fe, 0.02%Cr) and in Zircaloy-4 (0.2%Fe, 0.1%Cr) (see Table 1) were in the right proportion to explain the relative photocurrent values. This suggested that the observed contributions at low energy could correspond to additional Fe and Cr-containing oxides formed during the oxidation process. Using PEC results from previous studies on thermal scales grown on pure chromium or on ferritic steels [9,34–36] which are gathered in Table 3, we proposed to assign the low energy photocurrent spectrum to the presence of haematite $Fe_2O_3$ (region 2.2–2.6 eV), rhomboedric solid solution $(Fe_xCr_{1-x})_2O_3$ (region 2.6–3.0 eV) and chromia $Cr_2O_3$ (beyond 3.0 eV).

In order to confirm and to acquire additional information on the origin of the low energy contributions mentioned above, a microscopic study on

Table 3
Assignment of band-gap values to different iron and chromium oxide phases from [9,34–36]

| $Fe_2O_3$ | $(Fe_xCr_{1-x})_2O_3$ | $Cr_2O_3$ |
|---|---|---|
| $E_G \cong 2.2$ eV | $E_G \cong 2.6$ eV | $E_G \cong 3.0$ eV |

both samples using successive four increasing values of incident laser energy, allowing to detect $Fe_2O_3$ (2.41 eV), $(Fe_xCr_{1-x})_2O_3$ (2.73 eV) and $Cr_2O_3$ (3.51 eV and 3.72 eV) was performed.

PEC images recorded at 2.41 and 3.51 eV, with 2 μm resolution, on a $300 \times 300$ μm size area on the oxide grown on pure zirconium are presented in Fig. 6. In both images, the photocurrent values were very low, i.e. 2 nA, close to the average noise and consequently not relevant. Considering in addition that the macro PEC signal was clearly significant at the considered energies (Fig. 5), these images showed that iron and chromium oxide phases probably appeared as very small and homogeneously distributed precipitates in the zirconia matrix.

The PEC image recorded at 2.41 eV, with 3 μm resolution, on a $450 \times 450$ μm size area of oxide scale grown on Zircaloy-4 is presented in Fig. 7. This image is very different from the above described ones, revealing highly contrasted regions in photocurrent, with egg-shaped areas of size in the range 5–15 μm. According to the incident energy value, we associate these areas with the presence of Fe and Cr oxide precipitate clusters embedded in the zirconia matrix, considering that in the literature, the classical observed size of intermetallic diameter is about 300 nm. Following this first result, a set of high resolution PEC images ($220 \times 220$ μm) recorded at all available energies, from the right upper corner of the last image is presented in Fig. 8. Again, these images revealed well defined areas that can be classified into three types depending on their photocurrent evolution with energy. Type I, the most frequent is observed at 2.41 eV and progressively disappears at higher energies. According to the previous discussion, these areas should correspond to pure haematite $Fe_2O_3$. Type II corresponds to photocurrent nearly constant with energy. It might be associated with a mixture of $Fe_2O_3$, rhomboedric solid solution $(Fe_xCr_{1-x})_2O_3$ and $Cr_2O_3$ oxides. Type III, the most rare, corresponds to areas that appear at 3.51 eV and are clearly observed at 3.72 eV. It was associated with pure chromia $Cr_2O_3$. The local development of Fe and Cr oxide precipitates is in good agreement with the fact that iron and chromium present in Zircaloy-4 are known to form intermetallic Laves-phases $\gamma$-$Zr(Fe,Cr)_2$ [1–3,37]. Moreover, the detection of these three 'pure' phases in the zirconia matrix could be understood as the result of the successive oxidation of iron and chromium depending on the scale thickness and on the oxygen chemical potential value as it was showed by Pêcheur et al. [3]. However, we cannot totally exclude the presence of other semiconductor phases like $ZrFe_xCr_yO_z$ for which band-gaps are unknown.

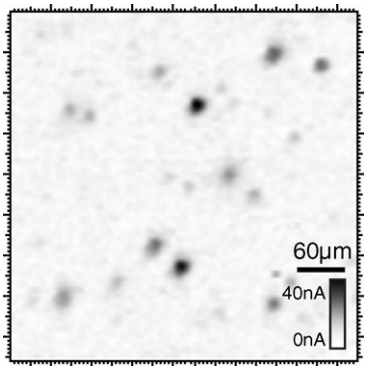


Fig. 7. PEC image of the oxide scale grown at 470 °C during 1 h in oxygen on Zircaloy-4 (applied potential: 0 V/MSE). Images $450 \times 450$ μm, point spacing 3 μm, laser energy 2.41 eV.

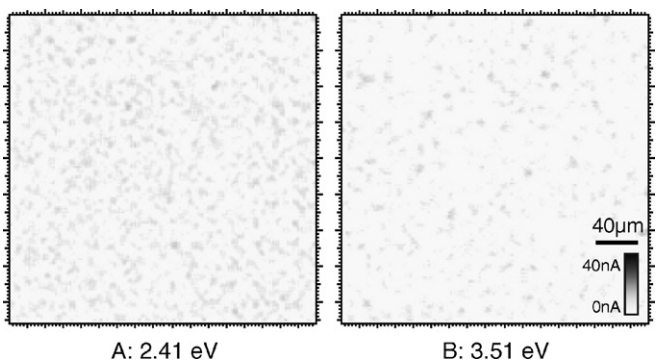


Fig. 6. PEC images of the oxide scale grown at 470 °C during 1 h in oxygen on 'pure' zirconium (applied potential: 0 V/MSE). Images $300 \times 300$ μm, point spacing 2 μm. A: laser energy 2.41 eV, B: laser energy 3.51 eV.

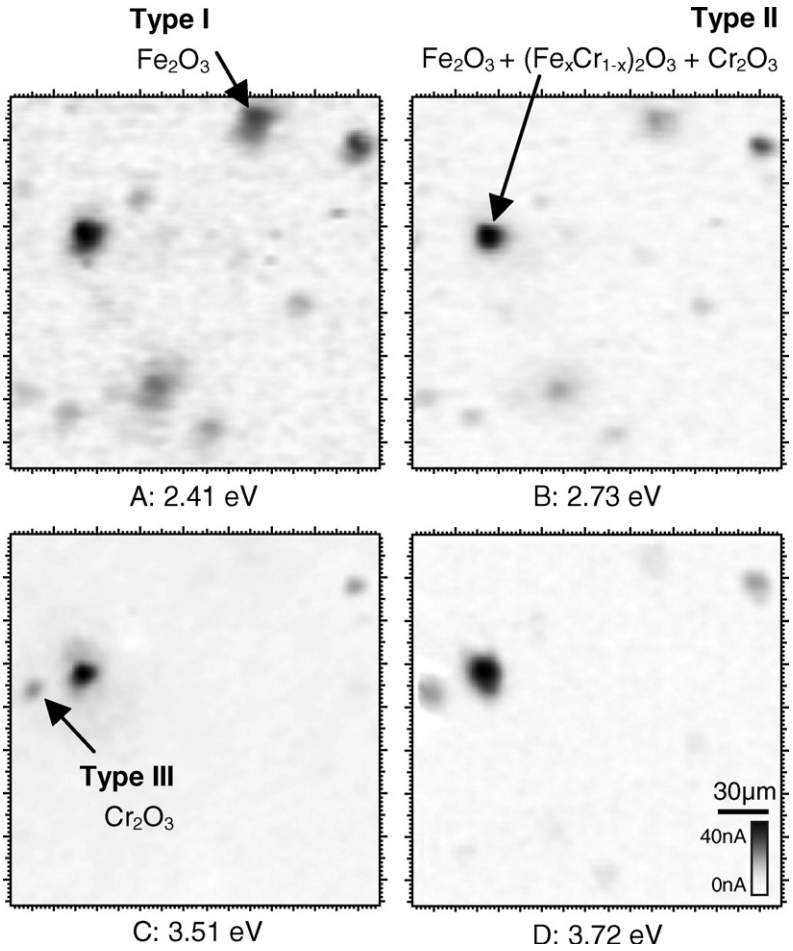


Fig. 8. PEC images of the oxide scale grown at 470 °C during 1 h in oxygen on Zircaloy-4 (applied potential: 0 V/MSE). Images $220 \times 220$ µm, point spacing 2 µm. A: laser energy 2.41 eV, B: laser energy 2.73 eV, C: laser energy 3.51 eV, D: laser energy 3.72 eV.

Thus, from these microscopic PEC images, it was demonstrated that the spatial distribution of various chromium and iron oxides in the zirconia matrix $ZrO_2$ can be studied very precisely.

Regarding others possible phases being able to account for low energy PEC contributions, in particular hydrated external phase such as $ZrO_2(H_2O)_n$, it must be pointed out that long time PEC image acquisition up to 15 h has never produced any photocurrent evolution neither in intensity nor in lateral distribution. Consequently, it was concluded that no detectable effect of progressive hydration with time took place as the oxide scale was exposed to aqueous electrolyte. Moreover, if low energy contributions were due to hydrated sub-scale as proposed in the literature [26,27], the specific spatial distributions of these ones observed at microscopic level could not be understood. Indeed, assumption of the development of network porosity perpendicular to the interface as proposed in the literature should induce an electrochemical short circuit and consequently the impossibility to measure any PEC signal. For these reasons, the proposition often found in previous studies involving the presence of an external hydrated layer producing a band-gap at low energies (2–4 eV) was not retained in the present case of scales grown at high temperature in pure oxygen.

Finally, regarding to the other impurities or addition elements such as Hf and Sn, we might expect to find also $HfO_2$ and $SnO_2$ oxides as a result of the oxidation process. Sn is typically observed in substitutional solid solution in zirconium alloys, with no evidence of metallic Sn or intermetallic $Zr_4Sn$ phases [38]. It would therefore lead to the formation of highly dispersed $SnO_2$ in zirconia. Our macro

PEC technique should detect this phase for which the accepted value of the direct band-gap transition is around 4 eV [39]. However, our micro PEC equipment would not give any results on the lateral distribution of this phase, considering that the highest available energy of the laser is 3.72 eV, lower than the band-gap or $SnO_2$. The other possible oxide, $HfO_2$, is known to exhibit a band-gap of 5.9 eV [32] and consequently should not be detected in both macro and micro experiments.

## 4. Conclusion and future directions

PhotoElectroChemical technique was shown to be a performing tool for assessing the nature and lateral distribution of semiconductor phases present in thermally grown oxide scales on zirconium materials. Macroscopic associated with microscopic PEC with control of incident laser beam energy allowed to effectively discriminate minor oxides in the $ZrO_2$ scale. In the case of Zircaloy-4, it was possible to clearly identify the presence and distribution of haematite $Fe_2O_3$, rhomboedric solid solution $(Fe_xCr_{1-x})_2O_3$, and chromia $Cr_2O_3$. At this time, no information on the amount, localisation in thickness and evolution with time of these oxides in the scale is available. It is expected to progress in the future by coupling micro PEC studies with kinetic experiments and with SEM techniques. It is also planned to lead micro Raman and XPS studies in order to complete our understanding of the effect of iron and chromium during the thermal oxidation of Zircaloy-4.

## References

[1] J.H. Baek, Y.H. Jeong, J. Nucl. Mater. 304 (2–3) (2002) 107.
[2] Y. Hatano, R. Hitaka, M. Sugisaki, M. Hayashi, J. Nucl. Mater. 248 (1) (1997) 311.
[3] D. Pêcheur, J. Nucl. Mater. 278 (2–3) (2000) 195.
[4] A.J. Nozik, Ann. Rev. Phys. Chem. 29 (1) (1978) 189.
[5] S. Maffi, C. Lenardi, B. Bozzini, L.P. Bicelli, Meas. Sci. Technol. 13 (2002) 1398.
[6] P. Clechet, C. Martelet, R. Olier, J.-P. Thomas, M.J. Fallavier, Electrochem. Soc. 130 (8) (1983) 1795.
[7] M. Arita, Y. Hayashi, Mater. Trans. 35 (4) (1994) 233.
[8] Y. Hayashi, M. Arita, K. Koga, M. Masuda, J. Alloys Comp. 231 (1) (1995) 702.
[9] A. Galerie, S. Henry, Y. Wouters, M. Mermoux, J.-P. Petit, L. Antoni, Mater. High Temp. 22 (1/2) (2005) 105.
[10] F. Di Quarto, S. Piazza, C. Sunseri, J. Electrochem. Soc. 130 (5) (1983) 1014.
[11] J.S.L. Leach, C.N. Panagopoulos, Electrochim. Acta. 31 (12) (1986) 1577.
[12] N. Khalil, A. Bowen, J.S.L. Leach, Electrochim. Acta. 33 (12) (1988) 1721.
[13] P. Meisterjahn, U. Konig, J.W. Schultze, Electrochim. Acta. 34 (4) (1989) 551.
[14] E.M. Patrito, R.M. Torresi, E.P.M. Leiva, V.A. Macagno, J. Electrochem. Soc. 137 (2) (1990) 524.
[15] M.J. Madou, K. Kinoshita, Electrochim. Acta. 29 (3) (1984) 411.
[16] J.H. Huot, J. Appl. Electrochem. 22 (9) (1992) 852.
[17] R.E. Salomon, W.M. Graven, G.B. Adams, J. Chem. Phys. 32 (1960) 310.
[18] E.M. Patrito, V.A. Macagno, J. Electrochem. Soc. 140 (1993) 1576.
[19] E.M. Patrito, V.A. Macagno, J. Electroanal. Chem. 371 (1–2) (1994) 59.
[20] R.A. Ploc, J. Nucl. Mater. 99 (1) (1981) 124.
[21] C.N. Panagopoulos, Mater. Lett. 3 (1985) 393.
[22] P. Meisterjahn, H.W. Hoppe, J.W. Schultze, J. Electroanal. Chem. 217 (1) (1987) 159.
[23] T.D. Burleigh, Corrosion 45 (1989) 464.
[24] A. Goossens, M. Vazquez, D.D. Macdonald, Electrochim. Acta 41 (1) (1996) 47.
[25] S. Preusser, U. Stimming, K. Wippermann, Electrochim. Acta 39 (8–9) (1994) 1273.
[26] F. Di Quarto, S. Piazza, C. Sunseri, M. Yang, S-M. Cai, Electrochim. Acta 41 (16) (1996) 2511.
[27] S. Lee, E. Cho, S. Ahn, H. Kwon, Electrochim. Acta 46 (17) (2001) 2605.
[28] J. Sánchez-González, A. Dıaz-Parralejo, A.L. Ortiz, F. Guiberteau, Appl. Surf. Sci. 252 (2006) 6013.
[29] S. Jana, P.K. Biswas, Mater. Lett. 30 (1997) 53.
[30] C. Kwok, C.R. Aita, J. Appl. Phys. 66 (6) (1989) 2756.
[31] S.R. Morisson, in: Electrochemistry at Semiconductor and Oxidized Metal Electrodes, Plenum Press, NY, 1986.
[32] D. Ciuparu, A. Ensuque, G. Shafeev, F. Bozon-Verduraz, J. Mater. Sci. Lett. 19 (11) (2000) 931.
[33] H.H. Kung, H.S. Jarett, A.W. Sleight, A. Ferreti, J. Appl. Phys. 48 (6) (1977) 2463.
[34] J.-P. Petit, M. Mermoux, Y. Wouters, A. Galerie, C. Chemarin, Mater. Sci. Forum. 461–464 (2004) 681.
[35] Y. Wouters, G. Bamba, A. Galerie, M. Mermoux, J.-P. Petit, Mater. Sci. Forum. 461–464 (2004) 839.
[36] S. Henry, J. Mougin, Y. Wouters, J.-P. Petit, A. Galerie, Mater. High Temp. 17 (2) (2000) 231.
[37] D.F. Taylor, H.R. Peters, W.J.S. Yang, in: Proceedings of the International Symposium on Environmental Degradation of Materials in Nuclear Power Systems-Water Reactors, 9th, Newport Beach, CA, United States, Aug. 1–5, 1999, p. 1161.
[38] A.J. Sawicki, J. Nucl. Mater. 264 (1–2) (1999) 169.
[39] G. Brankovic, Z. Brankovic, L.P.S. Santos, E. Longo, M.R. Davolos, J.A. Varela, Mater. Sci. Forum. 416–418 (2003) 651.